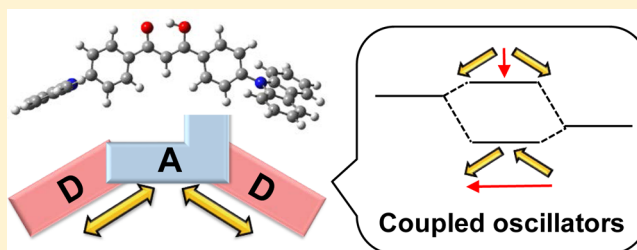


J-Type Heteroexciton Coupling Effect on an Asymmetric Donor–Acceptor–Donor-Type Fluorophore

Yuichi Kitagawa,^{*,†} Ryuto Yachi,[‡] Takayuki Nakanishi,[†] Koji Fushimi,[†] and Yasuchika Hasegawa^{*,†}[†]Faculty of Engineering, Hokkaido University, Kita-13 Jo, Nishi-8 Chome, Kita-ku, Sapporo, Hokkaido 060-8628, Japan[‡]Graduate School of Chemical Sciences and Engineering, Hokkaido University, Kita-13 Jo, Nishi-8 Chome, Kita-ku, Sapporo, Hokkaido 060-8628, Japan

Supporting Information

ABSTRACT: The novel donor–acceptor–donor (D–A–D)-type fluorophore with an asymmetric structure is reported. The twisted-induced charge transfer (TICT) luminescence was observed. The degree of charge transfer and radiative rate constant in the luminescence increased simultaneously with increase in orientational polarizability of solvents. In contrast to the numerous CT fluorophore researches, this behavior has never been previously observed. This characteristic behavior reveals the existence of an effective exciton coupling between the CT states in the donor–acceptor–donor-type fluorophore for the first time.



INTRODUCTION

Photosynthetic organisms have evolved a system for efficiently carrying out chemical reactions essential for supporting life activity on earth.^{1–4} This system is based on efficient light-harvesting, energy transfer, and charge-separated states originating from appropriate electronic structures and orientations of the molecules comprising photosynthetic organisms. Among these molecules, chlorosome, found in green sulfur bacteria, is a specific head-to-tail type aggregate (i.e., J-aggregates) with efficient light-harvesting and energy transfer characteristics.^{5–7} These excellent photophysical properties have motivated researchers to study the construction of artificial J-aggregates.^{8–17} Tamiaki and co-workers developed J-aggregates constructed from various organic-modified chlorophyll derivatives and successfully demonstrated their tunable light harvesting ability.^{8–11} This light sensitive J-aggregate showed remarkably efficient energy donor characteristics toward a titanium dioxide acceptor in dye-sensitized solar cells.¹² These efficient light-harvesting and energy donor properties are based on the J-type exciton coupling, which promotes the enhancement of the oscillator strength between the ground state (S_0) and the lowest singlet excited state (S_1).

The J-type exciton coupling with an enhanced oscillator strength is also expected to be of application in molecular designs for strong luminescent materials.^{13–17} In the field of “aggregation-induced emission (AIE)”, researchers have reported strong luminescence based on the induced large oscillator strength through J-aggregation.^{13–15} Recently, Lambert demonstrated an enhancement in luminescence using a small-size molecule with several heteroexcitons in the near excited energy level without J-aggregation.^{16,17} Thus,

effective enhanced luminescence was demonstrated using exciton coupling with large transition dipole moments.

In the field of biotechnology and optoelectronics, the design of strong fluorophores presenting charge transfer (CT) transitions have attracted considerable attention,^{18–23} although CT transition generally induces a weak dipole moment. In this article, the effect of J-type heteroexciton coupling between CT excited states of fluorophores is reported for the first time. To achieve effective J-type heteroexciton coupling, we applied asymmetric donor–acceptor–donor (D–A–D)-type structures (Figure 1a, As–D–A–D),^{24–27} which are expected to present two heteroexcitons. Specifically, carbazole (Figure 1b, D) and

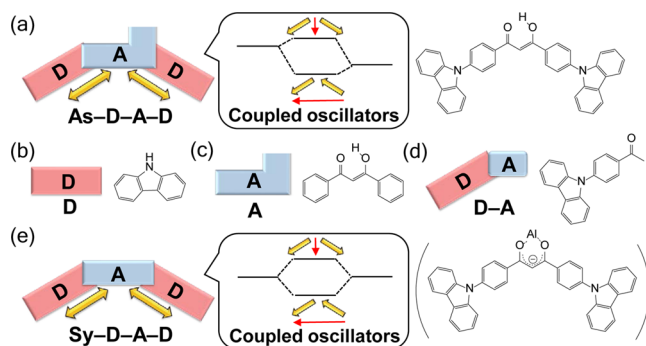


Figure 1. Chemical structures of As–D–A–D (a), D (b), A (c), D–A (d), and Sy–D–A–D (e).

Received: March 23, 2017

Revised: May 6, 2017

Published: June 5, 2017

dibenzoylmethane (Figure 1c, A) were used as a donor and an acceptor, respectively. We also prepared a D–A-type structure (Figure 1d) and the symmetrical D–A–D-type structure (Figure 1e, Sy–D–A–D) for comparison of the photophysical properties. The photophysical properties of the designed novel fluorophores were discussed in terms of exciton coupling.

EXPERIMENTAL SECTION

Apparatus. UV–vis absorption spectra were measured using a JASCO V-670 spectrophotometer. Fluorescence and excitation spectra were measured using an FP-6300 spectrofluorometer. Quantum yields were measured using an FP-6300 spectrofluorometer with an integration sphere. Fluorescence lifetimes were recorded on a picosecond fluorescence lifetime measurement system (C11200, Hamamatsu) equipped with picosecond light pulser (C10196), spectrograph (C11119–02), and streak scope (C10627). ^1H NMR spectra were recorded in CDCl_3 , CD_2Cl_2 , or $\text{DMSO}-d_6$ on a JEOL ECS-400 (400 MHz) spectrometer; CHCl_3 ($\delta_{\text{H}} = 7.26$ ppm), CH_2Cl_2 ($\delta_{\text{H}} = 5.32$ ppm), and DMSO ($\delta_{\text{H}} = 2.54$ ppm) were used as internal references, respectively. Electrospray ionization (ESI) mass spectrometry was performed on a JEOL JMS-T100 LP instrument. Elemental analyses were performed by MICRO CORDER JM10.

Materials. Sodium hydride (NaH, 55% dispersion in paraffin liquid) was purchased from Kanto Chemical Co., Inc. (Japan). Tetrahydrofuran, super dehydrated, with stabilizer (for Organic Synthesis), xylene, super dehydrated, with stabilizer (for Organic Synthesis), aluminum(III) chloride (Al(III)Cl_3 , 99.9%), hydrochloric acid (HCl, 6 mol/L), potassium carbonate (K_2CO_3 , anhydrous), palladium(II) acetate (Wako Special grade), tri-*t*-butylphosphine (10 wt % in hexane), hexane (spectroscopic grade), toluene (spectroscopic grade), chloroform (CHCl_3 , spectroscopic grade), dichloromethane (CH_2Cl_2 , spectroscopic grade), and cyclohexane (spectroscopic grade) were purchased from Wako Pure Chemical Industries, Ltd. (Japan). 4-Bromoacetophenone (>98.0%), carbazole (>96.0%), dibenzoylmethane (>98.0%), and ethyl 4-bromobenzoate (>98.0%) were purchased from Tokyo Chemical Industry Co., Ltd. (Japan).

Synthetic Schemes and Their Identifications. *1-[4-(9H-Carbazol-9-yl)phenyl]ethanone (D–A)*. The 1-[4-(9H-carbazol-9-yl)phenyl]ethanone was prepared according to previously reported procedures.²⁸ A solution of xylene, super dehydrated (20 mL), was added dropwise to a three-necked flask containing 4-bromoacetophenone (1.52 g, 7.67 mmol), carbazole (1.12 g, 6.70 mmol), K_2CO_3 (2.96 g, 21.4 mmol), palladium(II) acetate (small amount), and tri-*t*-butylphosphine (1.0 mL) under Ar. The reaction mixture was stirred for 40 h at 120 °C. The product was extracted with CH_2Cl_2 , and the extracts were washed three times with distilled water and subsequently dried over anhydrous MgSO_4 . The solvent was subsequently evaporated after which solid compounds were formed. The compounds were separated by silica gel chromatography (hexane/ $\text{CH}_2\text{Cl}_2 = 1:1$, $R_f = 0.45$), which resulted in a yellow compound.

Yield: 0.78 g (35.6%). ^1H NMR (400 MHz, CDCl_3 , TMS): δ /ppm = 2.70 (3H, s), 7.30–7.35 (2H, m), 7.41–7.52 (4H, m), 7.69–7.74 (2H, m), 8.14–8.16 (2H, d, $J = 8.0$ Hz), 8.19–8.24 (2H, d, $J = 8.8$ Hz).

4-(9H-Carbazol-9-yl) Benzoic Acid Ethyl Ester. The 4-(9H-carbazol-9-yl) benzoic acid ethyl ester was prepared according to previously reported procedures.²⁸ A solution of xylene, super

dehydrated (40 mL), was added dropwise to a three-necked flask containing ethyl 4-bromobenzoate (3.02 g, 13.3 mmol), carbazole (2.20 g, 13.1 mmol), K_2CO_3 (5.07 g, 36.7 mmol), palladium(II) acetate (small amount), and tri-*t*-butylphosphine (1.0 mL) and subsequently stirred for 48 h at 120 °C under Ar. The product was extracted with CH_2Cl_2 , and the extracts were washed three times with distilled water and subsequently dried over anhydrous MgSO_4 . The solvent was subsequently evaporated after which solid compounds were formed. The compounds were separated by silica gel chromatography (hexane: $\text{CH}_2\text{Cl}_2 = 1:1$, $R_f = 0.45$). The compound was washed with ethanol, and white solid was obtained.

Yield: 0.76 g (18.0%). ^1H NMR (400 MHz, CDCl_3 , TMS): δ /ppm = 1.40–1.50 (3H, m), 4.40–4.50 (2H, m), 7.29–7.36 (2H, m), 7.39–7.51 (4H, m), 7.67–7.72 (2H, m), 8.15 (2H, d, $J = 8$ Hz), 8.27–8.33 (2H, m).

1,3-Bis[4-(9H-carbazol-9-yl)phenyl]-1,3-propanedione (As–D–A–D). A solution of superdehydrated tetrahydrofuran (THF) (40 mL) was added dropwise to a three-necked flask containing 4-(9H-carbazol-9-yl) benzoic acid ethyl ester (0.76 g, 2.41 mmol) and NaH (0.40 g, 9.17 mmol) and subsequently stirred for 30 min under Ar. A solution of superdehydrated THF (20 mL) containing 1-[4-(9H-carbazol-9-yl)phenyl] ethanone (0.54 g, 1.90 mmol) was added dropwise to the above solution. The reaction mixture was stirred for 24 h at 60 °C. Water was added to the reaction mixture, which was neutralized by HCl (2 M). The product was extracted with CH_2Cl_2 , and the extracts were washed three times with distilled water and subsequently dried over anhydrous MgSO_4 . The solvent was subsequently evaporated after which solid compounds were formed. The compound was purified by reprecipitation (CH_2Cl_2 /hexane) and recrystallization (CH_2Cl_2 /hexane), which resulted in a brown solid compound.

Yield: 0.47 g (44.8%). ^1H NMR (400 MHz, CD_2Cl_2): δ /ppm = 7.08 (1H, s), 7.30–7.38 (4H, m), 7.42–7.50 (4H, m), 7.56 (4H, d, $J = 8.4$ Hz), 7.80 (4H, d, $J = 8.8$ Hz), 8.18 (4H, d, $J = 8.0$ Hz), 8.31 (4H, d, $J = 8.4$ Hz), 17.1 (1H, s). HRMS(ESI): found $m/z = 555.20$; calcd for $\text{C}_{39}\text{H}_{27}\text{N}_2\text{O}_2$: $[\text{M} + \text{H}]^+ = 555.20$.

Tris(1,3-bis[4-(9H-carbazol-9-yl)phenyl]-1,3-propanedione)aluminum (Sy–D–A–D). A solution of superdehydrated THF (20 mL) was added dropwise to a three-necked flask containing As–D–A–D (223.1 mg, 0.40 mmol), NaH (32.1 mg, 0.74 mmol), and Al(III)Cl_3 (21.2 mg, 0.16 mmol) and subsequently stirred for 60 h under Ar. The product was extracted with CH_2Cl_2 , and the extracts were washed three times with distilled water and subsequently dried over anhydrous MgSO_4 . The compound was purified by reprecipitation (CH_2Cl_2 /hexane) and recrystallization (THF) to form a yellow solid compound.

Yield: 132.8 mg (59.1%). ^1H NMR (400 MHz, CD_2Cl_2): δ /ppm = 7.26–7.35 (5H, m), 7.38–7.46 (4H, m), 7.53 (4H, d, $J = 8.4$ Hz), 7.77 (4H, d, $J = 8.4$ Hz), 8.14 (4H, d, $J = 8.0$ Hz), 8.46 (4H, d, $J = 8.8$ Hz). HRMS(ESI): found $m/z = 1133.36$; calcd for $\text{C}_{78}\text{H}_{50}\text{AlN}_4\text{O}_4$: $[\text{M}-\text{L}]^+ = 1133.36$. Elemental analysis: found, C 82.38%, H 4.63%, N 4.77%; calcd for $\text{C}_{117}\text{H}_{75}\text{AlN}_6\text{O}_6 + \text{H}_2\text{O}$: C 82.38%, H 4.55%, N 4.93%.

RESULTS AND DISCUSSION

As–D–A–D-Type Structure. β -Diketone derivatives generally exist in their keto and *cis*-enol forms in solution at room temperature.^{29,30} Here, we performed nuclear magnetic resonance (NMR) measurements for the analysis of keto–enol

ratio of As–D–A–D in solution. In this research, we used four solvents, hexane, toluene, CHCl_3 , and CH_2Cl_2 . Because the fraction of *cis*-enol form tends to increase as the solvent polarity decreases,³¹ the NMR spectrum was measured using CD_2Cl_2 . NMR peaks at 17.1 (–OH) and 7.1 ppm (–CH) produced by the *cis*-enol proton were observed (Figure S1), while the peak at around 3.5–4.5 ppm (keto, –CH₂) was not clearly observed. The NMR integration ratio indicated the existence of the keto-form (keto-form, 11%; enol-form, 89%). DFT calculations under vacuum condition also indicated that the energy of the enol-form was lower than that of the keto-form (Figure S2, $\Delta E = 302 \text{ cm}^{-1}$). In addition, the energy of the two *cis*-enol forms are equal and are present in equal amounts.³² These facts indicate that the ground-state structure of As–D–A–D in solution at room temperature is symmetric.

Ground State Properties of As–D–A–D and Sy–D–A–D. The electronic absorption spectrum of As–D–A–D is shown in Figure 2a. A sharp absorption band at around 290 nm

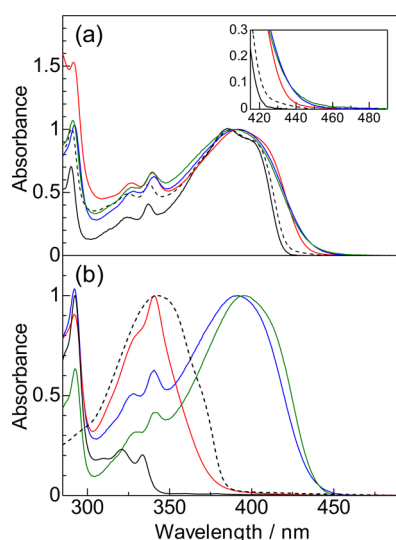


Figure 2. Solvent-dependent electronic absorption spectra (a) of As–D–A–D (cyclohexane, broken line; hexane, black line; toluene, red line; CHCl_3 , blue line; CH_2Cl_2 , green line). Electronic absorption spectra (b) of A (broken line), D (black line), D–A (red line), As–D–A–D (blue line), and Sy–D–A–D (green line) in CHCl_3 . Normalized by intensity maxima at the long or short wavelength bands.

and a broad band in 300–450 nm range were observed. As shown in the electronic absorption spectra in Figure 2b, the electronic absorption band at around 290 nm and the fraction of the broad band at short wavelengths are assigned to localized excited states of D and A moieties, respectively. The longest absorption edge (Figure 2a, inset) was slightly red-shifted as a result of the solvent polarity, suggesting that the transition band at the longest wavelength has a weak CT character. These absorption properties can be interpreted using DFT calculations (see Supporting Information). The relative absorption intensities around 290 and 330 nm were different depending on the type of solvent. The D–A (Figure 1d), which is expected to present an electronic structure similar to that of the keto-form, showed absorption bands at around 290 and 330 nm (Figure 2b). The differences in the relative intensity of these bands were produced by the different abundance ratio of the keto-form in each solvent. This interpretation was also

supported by the change in the electronic absorption underwent by the coordinated Al^{3+} (Sy–D–A–D, Figure 1e), which exhibited a lower relative absorption intensity at around 290 and 330 nm as compared to As–D–A–D (Figure 2b). In addition, coordination of Al^{3+} induced a red-shift in the broad absorption band.

Excited State Properties of As–D–A–D and Sy–D–A–D. The fluorescence spectra of As–D–A–D and Sy–D–A–D in various solvents ($\lambda_{\text{ex}} = 370 \text{ nm}$) are shown in Figure 3a,b, respectively. The fluorescence spectra of As–D–A–D

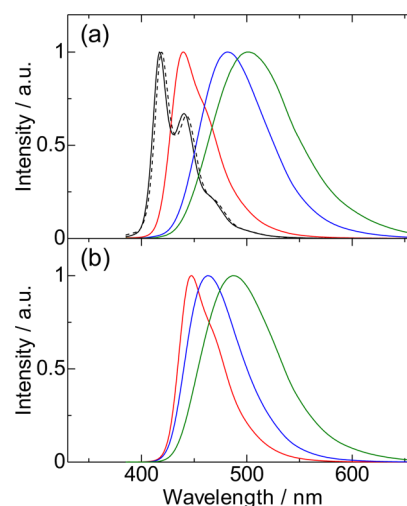


Figure 3. Solvent-dependent fluorescence spectra of As–D–A–D ((a) cyclohexane, broken line; hexane, black line; toluene, red line; CHCl_3 , blue line; CH_2Cl_2 , green line) and Sy–D–A–D ((b) toluene, red line; CHCl_3 , blue line; CH_2Cl_2 , green line). Normalized by intensity maxima.

were strongly red-shifted as a result of the orientational polarizability of the solvents (Δf),³³ which indicates the occurrence of twisted-induced charge transfer (TICT) fluorescence. The fluorescence bandwidth increased and the vibronic bands vanished with increase in Δf , thereby revealing an increase in the CT character with increase in Δf . A similar solvent-dependent behavior was observed for Sy–D–A–D, although its fluorescence bandwidth was larger than that of As–D–A–D in the same solvents (Figure 3 and Table 1), suggesting a lower CT degree of Sy–D–A–D as compared to As–D–A–D.

In order to clarify the excited state properties, we performed TD-DFT calculations for one of the As–D–A–D structures (*cis*-enol form and the S_1 state, Table S2). The optimized As–D–A–D structure showed different two-twisted angles between the A and the D moieties (Figure 4a). The luminescent state (S_1) was consistent with an HOMO \rightarrow LUMO excited electronic configuration. The HOMO is the localized orbital of the D moiety, which is strongly twisted (89.97°) from the A moiety (Figure 4b). The LUMO corresponds to the localized orbital of the A moiety (Figure 4b). This system induced strong CT transition with a significantly low oscillator strength ($f_{\text{osc}} < 0.0001$). The higher excited state (S_2) in the S_1 structure is consistent with a HOMO–1 \rightarrow LUMO excited electronic configuration. The HOMO–1 corresponds to a localized orbital of the D moiety, which is moderately twisted from the A moiety (69.16°) (Figure 4b). This moderate twisted angle induced a weaker CT

Table 1. Photophysical Parameter of As-D-A-D and Sy-D-A-D

	solvent	λ_{em}/nm (cm^{-1})	$\Phi_f/\%$ ^a	τ/ns ^b	k_r/s^{-1}	k_{nr}/s^{-1}	Δf	fwhm/ cm^{-1}
As-D-A-D	cyclohexane	419 (23,870)	0.41	3.6	1.1×10^6	2.8×10^8	-0.004	2120
As-D-A-D	hexane	417 (23,980)	0.99	3.5	2.8×10^6	2.8×10^8	0.001	2120
As-D-A-D	toluene	440 (22,730)	12.4	4.2	3.0×10^7	2.1×10^8	0.014	2290
As-D-A-D	CHCl ₃	482 (20,750)	44.4	3.0	1.5×10^8	1.9×10^8	0.150	3160
As-D-A-D	CH ₂ Cl ₂	500 (20,000)	46.6	4.9	9.5×10^7	1.1×10^8	0.220	3550
Sy-D-A-D	toluene	447 (22,370)	49.5	1.5	3.3×10^8	3.4×10^8	0.014	2160
Sy-D-A-D	CHCl ₃	463 (21,600)	55.9	2.7	2.1×10^8	1.6×10^8	0.150	2730
Sy-D-A-D	CH ₂ Cl ₂	487 (20,530)	60.0	4.1	1.5×10^8	9.8×10^7	0.220	3370

^a $\lambda_{ex} = 390$ nm. ^b $\lambda_{ex} = 380$ nm.

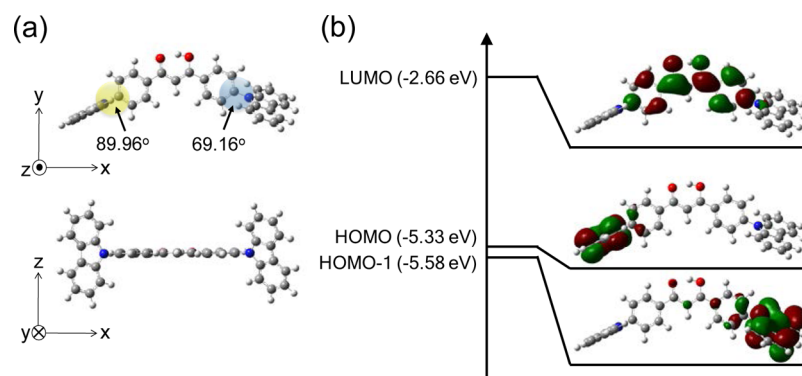


Figure 4. Optimized structure (a) and the molecular orbitals ((b) LUMO, HOMO, HOMO-1) for As-D-A-D.

transition with a large oscillator strength ($f_{osc} = 0.1220$). The higher excited states with large oscillator strengths are presented, which correspond to localized excited states of the A and D moieties (Table S2). These calculation results indicate that the actual luminescent states are primarily mixed with their excited states for As-D-A-D.

The photophysical parameters of As-D-A-D and Sy-D-A-D are shown in Table 1. In solvents with large Δf values (CHCl₃ and CH₂Cl₂), large fluorescence quantum yields were also observed despite the high degree of CT for As-D-A-D and Sy-D-A-D. These results can be explained in terms of the relatively large radiative rate constant (k_r) and small nonradiative rate constant (k_{nr}) for As-D-A-D and the relatively small k_{nr} for Sy-D-A-D at these conditions.

The k_{nr} is expressed as the sum of nonradiative rate constants from S_1 to S_0 (k_{vib}) and intersystem crossing constant from S_1 to T_n (k_{isc}). In general, high degree of CT and a low energy gap between S_1 and S_0 induce large k_{vib} . Here, we consider several intersystem crossing pathways. First, the ISC pathway between charge transfer excited states is considered. The high degree of CT induces a small energy gap between S_1 and T_n with CT, which is expected to induce the large k_{isc} . Second, the ISC between S_1 and the localized excited states of the A and D moieties is regarded. Previous reports suggest the localized triplet excited states of the A and D moieties to be 20,410 and 24,210 cm^{-1} , respectively.^{34,35} The luminescence energy of As-D-A-D in hexane, toluene, and CHCl₃ and that of Sy-D-A-D in toluene, CHCl₃, and CH₂Cl₂ were larger than that of the A moiety (Table 1), indicating potential ISC pathways between S_1 (CT) and the localized excited triplet state of the A moiety. Therefore, the large Δf value makes the suppressed intersystem crossing pathway with charge transfer between S_1 and the localized excited state, resulting in the small k_{nr} .

However, the k_r value increased for As-D-A-D and decreased for symmetric Sy-D-A-D with increase in Δf . In

the case of Sy-D-A-D, this behavior originates from the energy difference between the unchanged localized excited state and the changed excited degenerate CT state, depending on the solvents. The red-shifted luminescence in high polarity solvents induced large energy differences, which subsequently provided CT transition states with lower mixing for the localized excited states. This is a general phenomenon observed for CT luminescence.³³ In contrast, the radiative rate for As-D-A-D dependent on the solvent polarity is a unique phenomenon. The k_r constants tended to increase under the expected large energy difference between the lowest CT excited and the two localized excited states. These results indicate that the electronic coupling between the undegenerated CT excited states is an important factor for the interpretation of the photophysical behavior. To explain this unique phenomenon, we suggest the following models. When the CT degree of the S_1 state is large, the negative charge on the A moiety for the S_1 states is also large. This large negative charge imparts a larger twisted angle between the A and D moieties corresponding to the S_2 states. Therefore, near two twisted angles are produced, resulting in the lower energy difference between the S_1 and S_2 states, which is expected to induce effective exciton coupling between the two CT states.^{36,37} Thus, the k_r constants increased in solvents with large Δf values. Exciton coupling is one of the advantages of the stabilized S_n and unstabilized T_n states, which result in low S_1-T_1 energy gaps without decreasing the exchange integral related to the orbitals.³⁸ This phenomenon opens the possibility for synthesizing organic compounds with an inversion energy level between S_1 and T_1 (Figure S10). Further study on the relationship between S_1-T_1 energy and exciton coupling between CT excited states is now in progress.

CONCLUSIONS

In summary, we studied the photophysical properties of novel D–A–D molecules with asymmetric structure in terms of their heteroexciton coupling for the first time. These fluorophores exhibited specific luminescence properties originating from the exciton coupling between two CT states. These findings indicating effective exciton coupling between CT states open up new possibilities not only for the design of strong fluorophores presenting CT transition but also synthesis of the novel organic materials with an inversion energy level between S_1 and T_1 for high photostability and efficient electroluminescence without thermal-assisted delayed fluorescence.

ASSOCIATED CONTENT

Supporting Information

The Supporting Information is available free of charge on the ACS Publications website at DOI: 10.1021/acs.jpca.7b02783.

Al(III) A_3 , NMR spectrum, electronic absorption spectrum, and fluorescence spectrum of As–D–A–D, fluorescence spectra of A, D, and Al(III) A_3 , and DFT calculation details (PDF)

AUTHOR INFORMATION

Corresponding Authors

*E-mail: y-kitagawa@eng.hokudai.ac.jp.

*E-mail: hasegawa@eng.hokudai.ac.jp.

ORCID

Yuichi Kitagawa: 0000-0003-1487-2531

Yasuchika Hasegawa: 0000-0002-6622-8011

Notes

The authors declare no competing financial interest.

ACKNOWLEDGMENTS

This work was supported by the Matching Planner Program (Grant Number; MP28116808653) sponsored by the Japan Science and Technology Agency (JST).

REFERENCES

- (1) Blankenship, R. Early Evolution of Photosynthesis. *Plant Physiol.* **2010**, *154*, 434–438.
- (2) Gest, H. History of the Word Photosynthesis and Evolution of Its Definition. *Photosynth. Res.* **2002**, *73*, 7–10.
- (3) Witt, H. T.; Müller, A.; Rumberg, B. Electron-Transport System in Photosynthesis of Green Plants Analysed by Sensitive Flash Photometry. *Nature* **1963**, *197*, 987–991.
- (4) Croce, R.; van Amerongen, H. Natural Strategies for Photosynthetic Light Harvesting. *Nat. Chem. Biol.* **2014**, *10*, 492–501.
- (5) Huh, J.; Saikin, S. K.; Brookes, J. C.; Valleau, S.; Fujita, T.; Aspuru-Guzik, A. Atomistic Study of Energy Funneling in the Light-Harvesting Complex of Green Sulfur Bacteria. *J. Am. Chem. Soc.* **2014**, *136*, 2048–2057.
- (6) Borisov, A. Y. On the Efficiency of Energy Migration from the Chlorosome to the Main Bacteriochlorophyll in Green Bacteria. *Biophysics* **2012**, *57*, 163–165.
- (7) Günther, L. M.; Jendry, M.; Bloemsmas, E. A.; Tank, M.; Oostergetel, G. T.; Bryant, D. A.; Knoester, J.; Köhler, J. Structure of Light-Harvesting Aggregates in Individual Chlorosomes. *J. Phys. Chem. B* **2016**, *120*, 5367–5376.
- (8) Tamiaki, H.; Miyatake, T.; Tanikaga, R.; Holzwarth, A. R.; Schaffner, K. Self-Assembly of an Artificial Light-Harvesting Antenna: Energy Transfer from a Zinc Chlorin to a Bacteriochlorin in a

Supramolecular Aggregate. *Angew. Chem., Int. Ed. Engl.* **1996**, *35*, 772–774.

(9) Miyatake, T.; Tamiaki, H. Self-Aggregates of Natural Chlorophylls and Their Synthetic Analogues in Aqueous Media for Making Light-Harvesting Systems. *Coord. Chem. Rev.* **2010**, *254*, 2593–2602.

(10) Shoji, S.; Hashishin, T.; Tamiaki, H. Construction of Chlorosomal Rod Self-Aggregates in the Solid State on Any Substrates from Synthetic Chlorophyll Derivatives Possessing an Oligomethylene Chain at the 17-Propionate Residue. *Chem. - Eur. J.* **2012**, *18*, 13331–13341.

(11) Shoji, S.; Ogawa, T.; Hashishin, T.; Ogasawara, S.; Watanabe, H.; Usami, H.; Tamiaki, H. Nanotubes of Biomimetic Supramolecules Constructed by Synthetic Metal Chlorophyll Derivatives. *Nano Lett.* **2016**, *16*, 3650–3654.

(12) Wang, X.-F.; Wang, L.; Tamai, N.; Kitao, O.; Tamiaki, H.; Sasaki, S. Development of Solar Cells Based on Synthetic Near-Infrared Absorbing Purpurins: Observation of Multiple Electron Injection Pathways at Cyclic Tetrapyrrole–Semiconductor Interface. *J. Phys. Chem. C* **2011**, *115*, 24394–24402.

(13) Bui, H. T.; Kim, J.; Kim, H. J.; Cho, B.-K.; Cho, S. Advantages of Mobile Liquid-Crystal Phase of AIE Luminogens for Effective Solid-State Emission. *J. Phys. Chem. C* **2016**, *120*, 26695–26702.

(14) Tao, D.-D.; Wang, Q.; Yan, X.-S.; Chen, N.; Li, Z.; Jiang, Y. B. Ag⁺ Coordination Polymers of a Chiral Thiol Ligand Bearing an AIE Fluorophore. *Chem. Commun.* **2017**, *53*, 255–258.

(15) Choi, S.; Bouffard, J.; Kim, Y. Aggregation-Induced Emission Enhancement of a Meso-Trifluoromethyl BODIPY via J-aggregation. *Chem. Sci.* **2014**, *5*, 751–755.

(16) Lambert, C.; Scherpf, T.; Ceymann, H.; Schmiedel, A.; Holzappel, M. Coupled Oscillators for Tuning Fluorescence Properties of Squaraine Dyes. *J. Am. Chem. Soc.* **2015**, *137*, 3547–3557.

(17) Ceymann, H.; Balkenhohl, M.; Schmiedel, A.; Holzappel, M.; Lambert, C. Localised and Delocalised Excitons in Star-Like Squaraine Homo- and Heterotrimers. *Phys. Chem. Chem. Phys.* **2016**, *18*, 2646–2657.

(18) Uoyama, H.; Goushi, K.; Shizu, K.; Nomura, H.; Adachi, C. Highly Efficient Organic Light-Emitting Diodes from Delayed Fluorescence. *Nature* **2012**, *492*, 234–238.

(19) Nakanotani, H.; Higuchi, T.; Furukawa, T.; Masui, K.; Morimoto, K.; Numata, M.; Tanaka, H.; Sagara, Y.; Yasuda, T.; Adachi, C. High-Efficiency Organic Light-Emitting Diodes with Fluorescent Emitters. *Nat. Commun.* **2014**, *5*, 4016.

(20) Rajamalli, P.; Senthilkumar, N.; Gandeepan, P.; Huang, P.-Y.; Huang, M.-J.; Ren-Wu, C.-Z.; Yang, C.-Y.; Chiu, M.-J.; Chu, L.-K.; Lin, H.-W.; Cheng, C.-H. A New Molecular Design based on Thermally Activated Delayed Fluorescence for Highly Efficient Organic Light Emitting Diodes. *J. Am. Chem. Soc.* **2016**, *138*, 628–634.

(21) Seo, J.; Kim, S.; Park, S. Y. Strong Solvatochromic Fluorescence from the Intramolecular Charge-Transfer State Created by Excited-State Intramolecular Proton Transfer. *J. Am. Chem. Soc.* **2004**, *126*, 11154–11155.

(22) Bonn, A. G.; Wenger, O. S. Charge Transfer Emission in Oligotriarylamine-Triarylborane Systems. *J. Org. Chem.* **2015**, *80*, 4097–4107.

(23) Chen, W.; Zhang, Z. Y.; Li, X.; Agren, H.; Su, J. H. Highly Sensitive Detection of Low-Level Water Content in Organic Solvents and Cyanide in Aqueous Media Using Novel Solvatochromic AIEE Fluorophores. *RSC Adv.* **2015**, *5*, 12191–12201.

(24) Chignell, C. F.; Bilskj, P.; Reszka, K. J.; Motten, A. G.; Sik, R. H.; Dahl, T. A. Spectral and Photochemical Properties of Curcumin. *Photochem. Photobiol.* **1994**, *59*, 295–302.

(25) Barik, A.; Goel, N. K.; Priyadarsini, K. I.; Mohan, H. Effect of Deuterated Solvents on the Excited State Photophysical Properties of Curcumin. *J. Photosci.* **2004**, *11*, 95–99.

(26) Ghosh, R.; Mondal, J. A.; Palit, D. K. Ultrafast Dynamics of the Excited States of Curcumin in Solution. *J. Phys. Chem. B* **2010**, *114*, 12129–12143.

(27) Barik, A.; Indira Priyadarsini, K. Solvent Dependent Photo-physical Properties of Dimethoxy Curcumin. *Spectrochim. Acta, Part A* **2013**, *105*, 267–272.

(28) Watanabe, M.; Nishiyama, M.; Yamamoto, T.; Koie, Y. Palladium/ $P(t\text{-Bu})_3$ -Catalyzed Synthesis of N-Aryl Azoles and Application to the Synthesis of 4,4',4''-Tris(N-azolyl)triphenylamines. *Tetrahedron Lett.* **2000**, *41*, 481–483.

(29) Nie, D.; Bian, Z.; Yu, A.; Chen, Z.; Liu, Z.; Huang, C. Ground and Excited State Intramolecular Proton Transfer Controlled Intramolecular Charge Separation and Recombination: A New Type of Charge and Proton Transfer Reaction. *Chem. Phys.* **2008**, *348*, 181–186.

(30) Minoura, Y.; Nagashima, N.; Kudoh, S.; Nakata, M. Mechanism of UV-Induced Conformational Changes Among Enol-Type Isomers of (Trifluoroacetyl)acetone Studied by Low-Temperature Matrix-Isolation Infrared Spectroscopy and Density Functional Theory Calculation. *J. Phys. Chem. A* **2004**, *108*, 2353–2362.

(31) Emsley, J.; Freeman, N. J. β -diketone Interactions: Part 5. Solvent Effects on the Keto \rightleftharpoons Enol Equilibrium. *J. Mol. Struct.* **1987**, *161*, 193–204.

(32) Koltsov, A. I. Enol-Enol Tautomerism in Cis-Keto-Enols. *J. Mol. Struct.* **1998**, *444*, 1–11.

(33) Benniston, A. C.; Harriman, A.; Rostron, J. P. The Effect of Solvent Polarity on the Photophysical Properties of 4-cyano-(4'-methylthio)diphenylacetylene: A Prototypic Donor–Acceptor System. *Phys. Chem. Chem. Phys.* **2005**, *7*, 3041–3047.

(34) Castex, M. C.; Olivero, C.; Pichler, G.; Ades, D.; Siove, A. Fluorescence, Room Temperature Phosphorescence and Photodegradation of Carbazole Compounds in Irradiated Poly(methyl methacrylate) Matrices. *Synth. Met.* **2006**, *156*, 699–704.

(35) Yang, L.; Gong, Z.; Nie, D.; Lou, B.; Bian, Z.; Guan, M.; Huang, C.; Lee, H. J.; Baik, W. P. Promoting Near-Infrared Emission of Neodymium Complexes by Tuning the Singlet and Triplet Energy Levels of β -diketonates. *New J. Chem.* **2006**, *30*, 791–796.

(36) This electronic coupling occurs via vibronic and exciton couplings. The large distance between the two D moieties hinders vibronic coupling between the two CT excited states, which suggests that exciton coupling prevails.

(37) The k_r of As–D–A–D in CHCl_3 is larger than that in CH_2Cl_2 , due to reduced mixing with the localized excited states.

(38) Kitagawa, Y.; Hiromoto, H.; Ishii, K. Electronic Absorption, MCD, and Luminescence Properties of Porphyrin J-aggregates. *J. Porphyrins Phthalocyanines* **2013**, *17*, 703–711.